Icarus 308 (2018) 61–70

Contents lists available at ScienceDirect

Icarus

journal homepage: www.elsevier.com/locate/icarus

A search for polycyclic aromatic hydrocarbons over the Martian South Polar Residual Cap

J.D. Campbell*, P. Sidiropoulos, J-P. Muller

Imaging Group, Mullard Space Science Laboratory, University College London, Holmbury St Mary, Surrey RH5 6NT, UK

ARTICLE INFO

Article history:
Received 1 April 2017
Revised 29 January 2018
Accepted 8 March 2018
Available online 4 April 2018

ABSTRACT

We present our research on compositional mapping of the Martian South Polar Residual Cap (SPRC), especially the detection of organic signatures within the dust content of the ice, based on hyperspectral data analysis. The SPRC is the main region of interest for this investigation, because of the unique CO_2 ice sublimation features that cover the surface. These flat floored, circular depressions are highly dynamic, and we infer frequently expose dust particles previously trapped within the ice during the wintertime. Here we identify suitable regions for potential dust exposure on the SPRC, and utilise data from the Compact Reconnaissance Imaging Spectrometer for Mars (CRISM) on board NASA's Mars Reconnaissance Orbiter (MRO) satellite to examine infrared spectra of dark regions assumed to be composed mainly of dust particles to establish their mineral composition, to eliminate the effects of ices on sub-pixel dusty features, and to look for signatures indicative of Polycyclic Aromatic Hydrocarbons (PAHs). Spectral mapping has identified compositional differences between depression rims and the majority of the SPRC and CRISM spectra have been corrected to minimise the influence of CO_2 ice. Whilst no conclusive evidence for PAHs has been found within the detectability limits of the CRISM instrument, depression rims are shown to have higher water content than regions of featureless ice, and there are possible indications of magnesium carbonate within the dark, dusty regions.

1. Introduction

Mars has long been the subject of scientific exploration, with a focus on investigations of conditions on ancient Mars, evidence of life, and the search for habitable environments (Fairén et al., 2010). During the last few decades, the polar regions have emerged as regions with increased scientific interest. Mars' polar regions, both in the northern and southern hemispheres, have residual caps that survive throughout each hemisphere's respective summer; the North Polar Residual Cap (NPRC) registers as predominately water ice, while the longer, colder winter in the southern hemisphere due to the orbit obliquity means that the South Polar Residual Cap is largely composed of CO_2 ice (Titus et al., 2003; Byrne, 2009) which overlays, and is surrounded by, water ice layers known as Polar Layered Deposits (PLD; Paige et al., 1990; Piqueux et al., 2008).

While the Martian climate may have been more 'Earth-like' in the past, with warmer, wetter conditions and an active magnetosphere (Fassett and Head, 2010), conditions on present day Mars are much less habitable. The attenuation of Mars' magnetosphere led to a loss of atmosphere through solar wind interactions, leaving the average temperatures and atmospheric surface pressures much lower than on the Earth (Johnson et al., 1996; Kass and Yung, 1995; Melosh and Vickery, 1989). Liquid water generally cannot exist on the surface of Mars due to low atmospheric temperatures and pressures and both water and CO_2 ice sublimate directly from the solid to vapour phase (Blackburn et al., 2010). The lack of a significant atmosphere on present-day Mars means that the surface is exposed to high levels of UV radiation, which would have a deleterious effect on any biological material on the planetary surface (Cockell et al., 2000);

However, the annual, seasonal sublimation and deposition of CO_2 ice on the SPRC leads to an unique surface feature known broadly as 'Swiss Cheese Terrain' (SCT), characterised by flat floored, circular depressions that can intersect to form intricate patterns reminiscent of Emmental Swiss Cheese (Malin et al., 2001). The SCT features are of particular interest as their seasonal sublimation cycles expose material previously shielded within the SPRC (Jian and Ip, 2009). More specifically, it would be of great interest to examine evidence of one particular class of organic molecules, Polycyclic Aromatic Hydrocarbons (PAHs), that may have been afforded protection from harmful radiation within the

* Corresponding author.
E-mail addresses: jacqueline.campbell.16@ucl.ac.uk (J.D. Campbell), p.sidiropoulos@ucl.ac.uk (P. Sidiropoulos), j.muller@ucl.ac.uk (J-P. Muller).

https://doi.org/10.1016/j.icarus.2018.03.008
0019-1035/

SPRC (Dartnell et al., 2012). While any dust trapped within the SPRC may have undergone past exposure during the geological history of Mars, there are potential mechanisms for present day sources of PAHs. In addition, as the evolution of the SPRC is still not well understood, it is worthwhile attempting to ascertain the sensitivity of instruments to possible PAH signatures, and the difficulties posed by overwhelming CO_2 signatures when analysing the SPRC in short-wave infrared wavelengths.

The detection of organics has been a primary objective of missions since the Viking missions Klein, 1978). Despite apparently negative results on the detection of extant life by the Viking landers in the 1970s, which searched for traces of biologically important compounds (Klein, 1978; Schuerger and Clark, 2007), perchlorates were discovered by the 2008 Phoenix lander (Hecht et al., 2009). More recently, organics were discovered by the Sample Analysis at Mars (SAM) instrument on NASA's 2011 rover mission, Mars Science Laboratory (Freissinet et al., 2015). Perhaps of even more interest, the reanalysis of the 1976 Viking Lander data by Navarro-Gonzalez et al. (2010) using modern techniques suggested there were both perchlorates and organic carbon present at the Viking Lander sample sites, although they were not identified at the time.

The identification of organic material can be done through the analysis of reflectance spectrometer data in order to establish compositional characteristics of the Martian surface. The use of spectrometers started in 1969, with Mariners 6 and 7 (Herr et al., 1972). Regarding SPRC dust, a first analysis was conducted by Douté et al. (2007). This work used data from the Mars Express instrument Observatoire pour la Minéralogie, l'Eau, les Glaces et l'Activité (OMEGA). The spatial resolution limitations of OMEGA (300 m–2 km/pixel; Bibring et al., 2004) mean that Douté et al.'s study of the SPRC was not able to resolve fine scale features.

Since the aim of our work is to look for regions of interest that might provide protection for fragile organic molecules, but also allow periodic exposure in order to be detectable on the SPRC from orbit, a finer spatial resolution than OMEGA is required, as SCT scarp walls are on a scale of 10s–100s of metres (Thomas et al., 2009). As a result, we use data from the Compact Reconnaissance Imaging Spectrometer for Mars (CRISM) on board NASA's Mars Reconnaissance Orbiter (MRO), which attains surface spatial resolution of ~20 m/pixel (Murchie et al., 2007). Using CRISM allows local analysis of regions of the SPRC with various morphologies, and in particular, thin dust rim features.

The rest of this paper is structured as follows; a brief analysis of the SPRC morphology and the importance of PAHs to astrobiology is given in Section 2, before passing to the presentation of the methods used in order to select regions of interest and carry out compositional mapping (Sections 3 and 4, respectively), and to the discussion of the achieved results (Section 5). Section 6 concludes this work.

2. Background

2.1. Martian South Polar Residual Cap

NASA's CTX Context Camera on board MRO has attained complete summer coverage of the SPRC with a spatial resolution of ~6 m/pixel, allowing detailed mapping of the various units of the entire polar cap (Thomas et al., 2009). The dynamic nature of the SPRC has been established by comparing current maps made from CTX imagery to earlier images from the Mars Orbital Camera (MOC) on Mars Global Surveyor, and by comparing images obtained during different orbits from the High Resolution Imaging Science Experiment (HiRISE) on board MRO (Thomas et al., 2005; Pommerol et al., 2011) (Fig. 1).

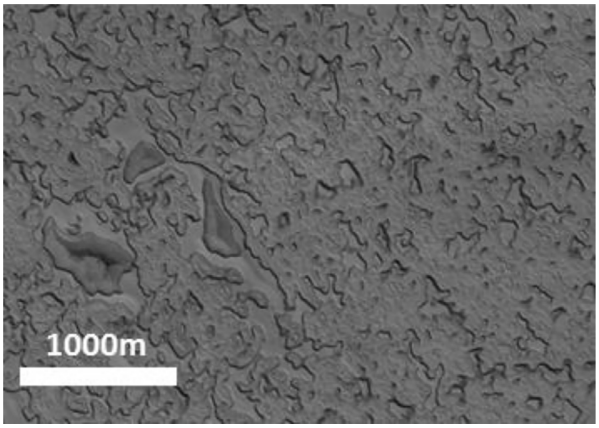

Fig. 1. Swiss Cheese Terrain (HiRISE image ESP_014380_0945).

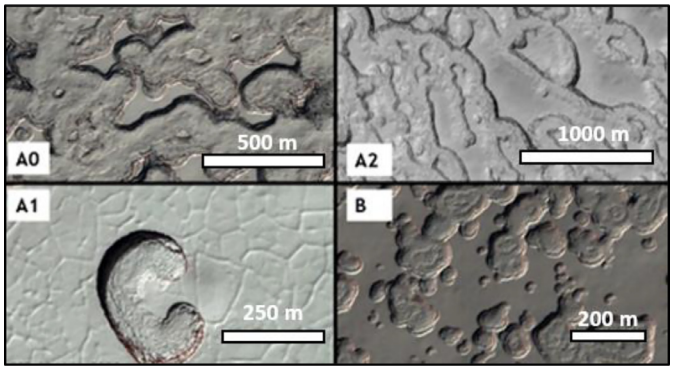

Fig. 2. Examples of SCT feature morphologies. HiRISE product IDs clockwise from top left: ESP_014380_0945, PSP_005386_0930, ESP_012271_0940, ESP_014141_0930. Morphology designations A0-B follow the terminology of Thomas et al. (2009).

The SPRC exhibits a range of morphologies. Fig. 2 shows some of the different features and textures that are informally grouped under the term SCT.

The SPRC consists of two distinct units; the upper unit (B) is made up of a series of 1–2 m thick layers superposed over a lower, older, thicker 10–14 m unit (A) that has undergone significant erosion (Thomas et al., 2005). The characteristics of the different SPRC morphologies are summarised in Table 1 (adapted from Thomas et al., 2005, 2009).

While there is evidence of vertical erosion or 'down-wasting', into the depression floors (Thomas et al., 2005) the majority of erosion occurs through lateral scarp retreat of depression walls (Byrne et al., 2008). The depression features within the lower, older unit exhibit a scarp retreat rate of ~3 m/MY, while the younger layers show scarp retreat rates of 2.2 m/MY (Thomas et al., 2009).

The surface layer of the SPRC predominantly registered as CO_2 ice when analysed using either THEMIS or OMEGA spectrometers, with depressions and SPRC edges exposing a small amount of water ice beneath (Bibring et al., 2004; Titus et al., 2003). The strongest signatures for water ice originate from around the margins of the SPRC (Titus et al., 2006). It is the retreating walls of depression features and floors of these depressions containing dark materials that are the principal study sites of our analysis in order to examine dust exposed on scarp features; regions of flat, high albedo ice on mesas and featureless terrain are also examined for contrast to establish the impact of dusty rims on spectra obtained using the CRISM instrument.

Table 1
Attributes of SPRC Terrain Units (based on Thomas et al. (2005, 2009).

Unit	Features
A0	Quasi-circular depressions >500 m diameter <1% of surface ~10–14 m thick
A1	Curl or heart-shaped depressions ~200 m diameter
A2	'Fingerprint' terrain: elongate, asymmetric depressions. Merges into unit A1 60–120 m across
B	Wide range of surface morphologies, but mostly circular depression features ranging from 10 s to 100 s of metres diameter. ~1 m thick layers overlying Unit A terrain

2.2. The importance of polycyclic aromatic hydrocarbons (PAHs) in astrobiology

PAHs are a group of chemical compounds consisting of benzene rings of hydrogen and carbon that are particularly stable compared to aliphatic (non-ring-like) hydrogen-carbon molecules (Carey, 2006).

PAHs occur on Earth as a result of incomplete combustion of organic material (Samanta et al., 2002), but have also been found to coalesce in space within dust clouds. Spectral signatures indicative of PAHs anthracene ($C_{14}H_{10}$) and pyrene ($C_{16}H_{10}$) were detected by Mulas et al. (2005) during their investigation of infrared emissions from the Red Rectangle Nebula. There are close to 120 known interstellar PAH species, which may account for up to 20% of total cosmic carbon (Allamandola, 2011).

PAHs formed in nebulae may rain down on primordial planets directly from planetary accretion discs, or can be delivered on comets and meteorites (Allamandola, 2011). PAHs can form in situ on planetary bodies through Fischer–Tropsch reactions of hydrogen and carbon-monoxide rich igneous material (Zolotov and Shock, 1999). Therefore, PAHs should be present, or have been present in the past, on all planetary bodies in the solar system (Dullemond et al., 2007).

Concentrations of over 1000 ppm of aromatic hydrocarbons have been found in carbonaceous chondrite meteorites (Botta and Bada, 2002), yet no PAHs have ever been detected on Mars. It is likely that PAHs on the surface would be rapidly destroyed by exposure to UV radiation or chemical reactivity of the Martian regolith (Quinn and Zent 1999; Benner and Devine, 2000). Following experiments in 'Mars chambers' that emulate environmental conditions on Mars, Dartnell et al. (2012) found that PAHs can be destroyed by exposure to UV radiation in as little as 3 days.

The presence of PAHs could indicate the degradation of organisms (Mckay and Gibson, 1996) and could therefore be a biomarker for extinct or even extant life. PAHs have not thus far been detected on Mars (Benner and Devine, 2000).

Dartnell et al. (2012) propose that PAHs might be protected from the deleterious effects of UV radiation and oxidization chemistry if they were within the subsurface of Mars, inside rock, or in areas of permanent shadow. Additionally, ice can act as a barrier to solar radiation (Vincent et al., 1998; Cockell et al., 2000), and allow organic compounds to become more complex where partial shielding of UV radiation occurs (Herbst and van Dishoek, 2009; Oberg et al., 2009). In situ astrobiological detection of the subsurface will be carried out in the future, for example on the ESA ExoMars Rover mission scheduled for launch in 2020, which will carry with it a drill unit capable of penetrating down to 2 m in depth (ESA, 2014). Until such times, remote sensing technology can be used to look for regions on Mars in which material previously shielded from UV has been uncovered by natural processes, such as sublimation in the South Polar Residual Cap (SPRC).

2.3. Detection of PAHs

Detection of PAHs outside Earth has been performed for many years. Spectral signatures in interstellar regions were first attributed to PAHs in the mid-1980s (Leger and Puget, 1984; Allamandola et al., 1985). The PAH diagnostic signature at 3.29 μm and its accompanying weaker bands and underlying structures between 3.1 and 3.7 μm (Tokunga et al., 1991) are of interest to this investigation due to the spectral range covered by the CRISM instrument.

PAHs have only been detected on a small number of solar system satellites, and comet 67P (Cruikshank et al., 2014; Davidsson et al., 2016). Spectral signatures indicative of PAHs have been found on the surfaces of two of Saturn's icy moons, Iapetus and Phoebe (Cruikshank et al., 2008; Cruikshank et al., 2014), and in the upper atmosphere of Saturn's moon Titan (Lopez-Puertas et al., 2013). Cruikshank et al. (2008, 2014) identified some of the organic material as PAHs based on spectral comparisons with the averaged spectral profiles of 6 astrobiologically significant PAHs (Colangeli et al., 1992) measured in laboratories (chrysene, triphenylene, perylene, benzo (α) pyrene, pentacene and coronene) with different water ice and tholene mixtures.

Unlike on the Martian SPRC, Iapetus and Phoebe have extensive, uninterrupted areas of dark material that mask the effects of ice on IR spectra.

3. Selecting regions of interest

We consider only Full Resolution Targeted products covering SCT, CRISM's highest spatial resolution mode (~20 m/pixel) for analysing rim features. 55 FRT scenes were divided into 13 separate groups, that each covers a corresponding SPRC region-of-interest with multiple products, acquired between 2007 and 2011 shown in Fig. 3.

The CRISM footprints were further narrowed down to those taken only in 2007 (MY 27), in order to capitalise on the most effective operating period of the CRISM instrument, and ensure similar Martian spring/summer environmental conditions. This resulted in 13 images ready to be processed and used for initial spectral analysis. RGB composites were generated for the 13 sites, and those that showed rim regions with the strongest spectral response for carbonate overtone-like properties were chosen (see Section 4.3 for description of how RGB composites were generated). Following this process, 5 sites were selected for further analysis (see Table 2, Fig. 4).

Table 2
Details of 5 CRISM scene sites.

Site no.	Product ID	Acquisition date	Lat.	Long.
1	FRT00007E26	26/09/2007	−84.9	298.4
2	FRT00006EEE	04/09/2007	−85.5	284.7
3	FRT00007CE5	21/09/2007	−86.8	297.8
4	FRT00005AE3	14/05/2007	−87.0	354.2
5	FRT000075F0	29/08/2007	−86.9	359.2

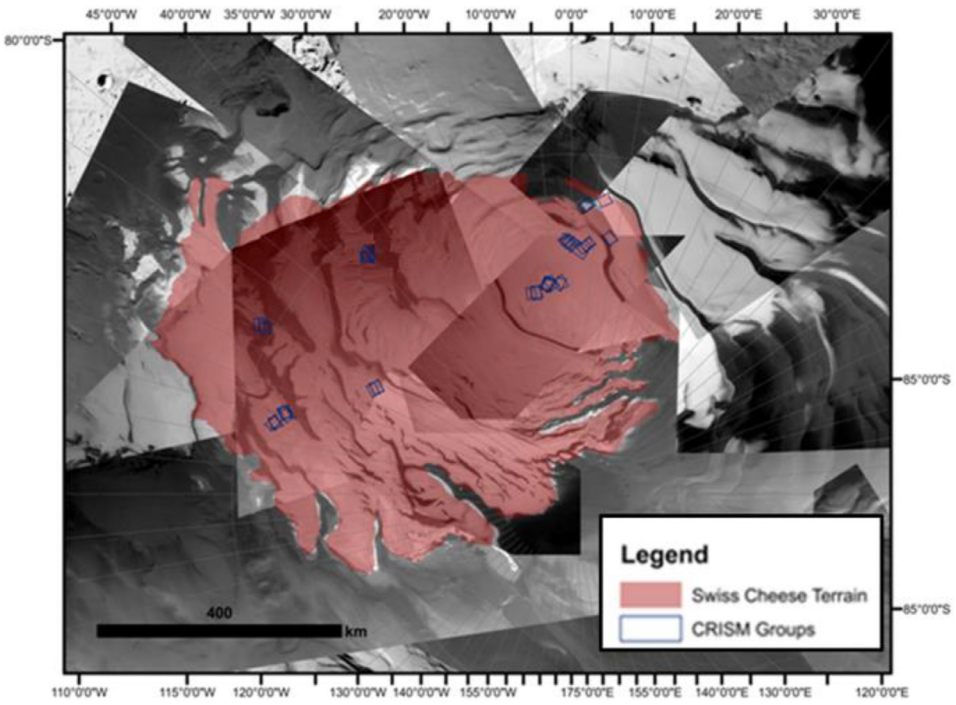

Fig. 3. Polar stereographic map of the Martian SPRC using a manually generated mosaic of HRSC images, showing 13 CRISM groups of interest (blue highlighted boxes). (For interpretation of the references to colour in this figure legend, the reader is referred to the web version of this article.)

- Site 1 is located at the edge of the SPRC and covers Unit B morphology.
- Site 2 is situated near the edge of the SPRC but does not include any ice-free surfaces, and covers Unit A0 and Unit B SPRC morphology
- Site 3 is located closer to the South Pole, well within the limits of the SPRC, and exhibits Unit A0 and B morphology.
- Site 4 is covered by characteristic 'curl features' of Unit A1.
- Site 5 covers Unit A0 and A2 morphology and is situated near the South Pole, adjacent to Site 4, supporting the idea that Unit A1 and A2 features represent different stages of the same sublimation morphology.

From these 5 sites, more specific regions of interest were chosen by looking at the spectral maps, and selecting rim features that showed a strong spectral response for carbonate overtone-like signatures, as well as regions that showed a strong response for H_2O and CO_2 ice for comparison.

4. Data and tools

4.1. Compact reconnaissance imaging spectrometer for Mars

Since MRO's mission objective is to study the history of water on Mars, among other instruments, it carries on-board the CRISM instrument (NASA, 2016). CRISM is a visible to infrared hyperspectral imager, capable of producing visible and infrared spectral profiles of Mars. One of CRISM's main objectives is to map key areas of mineralogical interest using targeted mode, (<1% surface coverage) at a spatial resolution of ~20 m/pixel, and spectral range of 362–3920 nm for 545 channels at a nominal spectral resolution of 6.55 nm/channel. This objective is very relevant to our research as the narrower spectral channels are required to be sensitive enough to pick out subtle spectral features, and the higher spatial resolution is needed to resolve the small-scale depression rim features. It should be noted that spectra obtained at wavelengths higher than 2.6 µm by CRISM are prone to noise, and therefore not ideal in identifying features in this spectral region, but are the only option for analysing fine scale features using SWIR in this spectral range.

Even though CRISM was not designed with the identification of organics as a primary objective, the large number of channels allows high sensitivity to carbonates (Murchie et al., 2007), which can be used to identify signatures that contain features indicative of carbonate overtones. For example, Pelkey et al. (2007) devised 44 spectral 'summary products' by using 'band math', where different bands are combined mathematically to develop a new band that is then diagnostic of particular compositions; this new band can then be used as a targeting tool to identify areas of mineralogical interest for further detailed analysis. It should be noted that these summary products do not definitively identify a particular mineralogy; they are simply a tool for distinguishing spectral signatures that match specific features of a particular mineralogy.

For the purposes of this investigation, the images with the highest spatial resolution are required in order to resolve small scale features of depression scarps; therefore, images obtained using Full Resolution Targeted (FRT) mode are used (with resolution ~20 m/pixel). It should be noted that CRISM, similar to all space instrumentation protected from the effects of the sun using cryogenic systems, is slowly getting warmer, decreasing the reliability of the instrument (Murchie et al., 2007). Consequently, only data acquired before 2011 are employed in our analysis.

4.2. Data calibration and pre-processing

The Harris ENVI + IDL® image processing software was used for calibration, pre-processing and analysis of the data, additionally using the CRISM Analysis Tool[1] plug-in when required. The image processing pipeline was based on "best practices" guides, which were released in the CRISM Data User's Workshop (Morgan et al., 2009).

[1] http://geo.pds.nasa.gov/missions/mro/crism.htm#Tools.

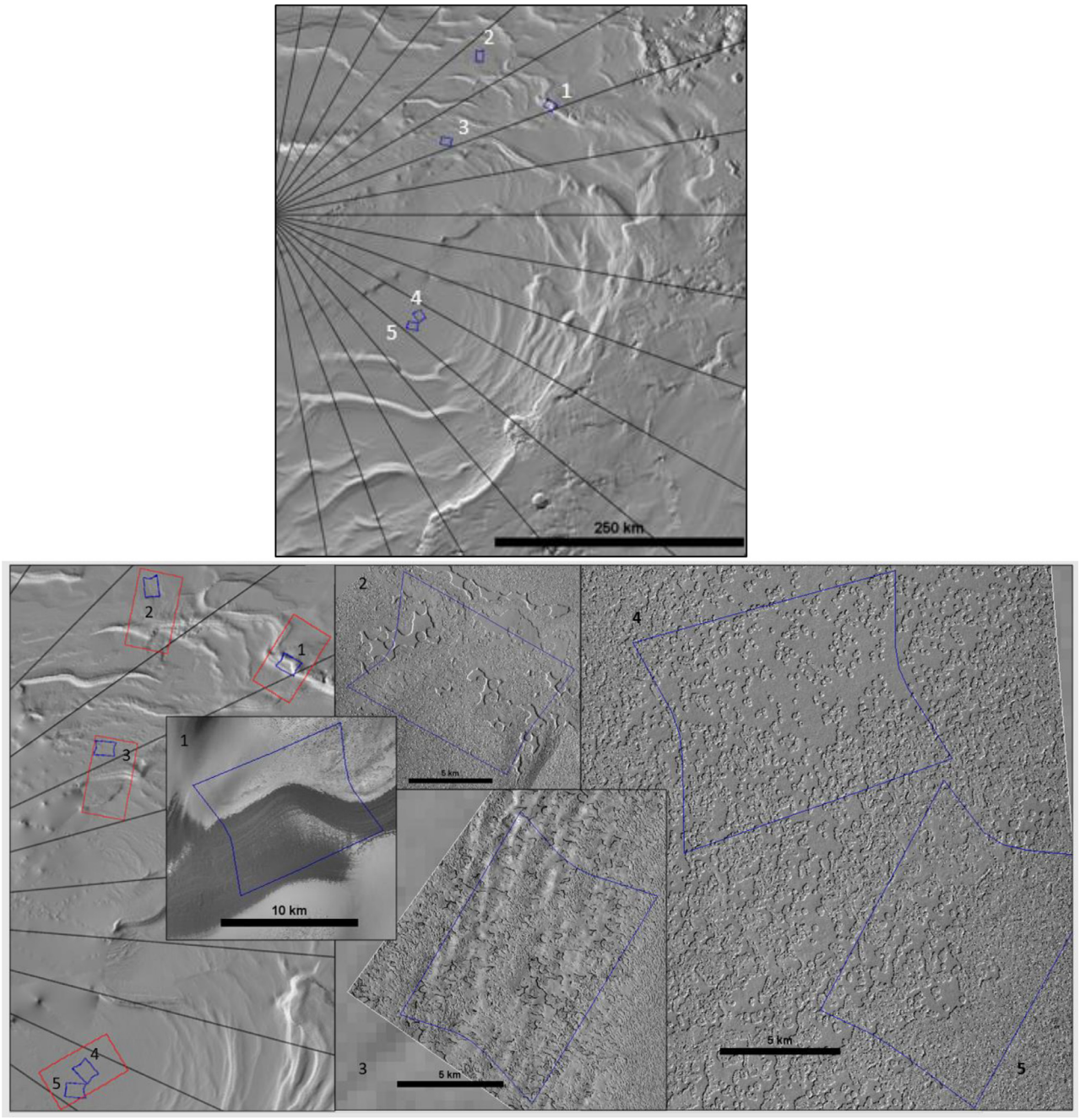

Fig. 4. Locations of 5 CRISM sites (top), with CTX imagery to show morphology (bottom): Site 1: CTX B11_014076_0952_XN_84S061W. Site 2: CTX B05_011756_0944_XN_85S074W. Site 3: B11_014090_0932_XI_86S057W. Sites 4 and 5: CTX B07_012374_0931_XN_86S006W.

More specifically, after ingestion into CAT_ENVI, radiance was converted to bi-directional reflectance factor to minimise the effects of different angles and levels of solar illumination. This 'photometric correction' employed a simple normalisation step, which was done by dividing by the cosine of the incidence angle (Africano et al., 2005). Atmospheric correction is then carried out using 'division by scaled volcano', i.e. by dividing the readings from the image being processed by the ratio of the highest altitude point on Mars (the summit of *Olympus Mons*, ~22 km) and its base, then multiply by a factor dependent on the altitude and season of image acquisition in order to remove the effects of atmospheric gases from spectra (Wiseman et al., 2016). Finally, destriping and despiking is used to remove residual artefacts from the imagery, as well as anomalous spikes in the spectra. However, it does not remove any of the 'no data' values; therefore, these need to be removed manually in a post-processing step, after spectra have been acquired. Once correction is completed, diagnostic summary products are generated.

4.3. Spectral mapping of CRISM scenes

Summary products are the input to the next stage of the processing, where spectral mapping is conducted on the CRISM products to identify those with the best spectral responses indicating possible carbonate overtones in regions on depression feature rims. Three of the aforementioned Pelkey (2007) summary products were applied to the images, each one stored in a different channel of a pseudo-RGB image, referred to here as a *RGB compos-*

ite summary. The products with weak spectral responses for carbonates on depression rims were rejected for further analysis. The employed summary products are:

- BD1435; diagnostic of CO_2 ice; displayed on the red channel
- BD1500; diagnostic of H_2O ice; displayed on the green channel
- BDCARB; diagnostic of carbonate overtones; displayed on the blue channel

These three were chosen in order to highlight the two most abundant units on the SPRC (CO_2 and water ice) and to identify any regions that may contain carbonates and with significant spectral differences to the (CO_2 and water) ice signatures. While the BDCARB summary product corresponds to different μm band depth than PAHs, it is a useful tool for highlighting differences in spectral reflectance. The band 'BDCARB' is diagnostic of carbonate overtone-like signatures, giving the strongest response where it detects spectral features similar to those observed when the vibrational spectrum of a carbonate molecule transitions from a ground to an excited state (Gaffey, 1986). The RGB composite summary product arrangement means the areas with a spectral response indicative of CO_2 ice show up as red, H_2O ice as green, and carbonate overtones as blue; blends show up as mixtures of these colours. Again, it is important to note that blue colours do not indicate definitive carbonate content, but this method certainly differentiates areas with varying spectral responses from each other.

Moreover, in order to allow the visual inspection of the morphological features of each CRISM scene, the original CRISM data have been used to create a second composite image, using RGB bands close to the default (in ENVI) bands, i.e. bands 230 (2509.7 nm), 75 (1486.9 nm) and 10 (1060.3 nm) for red, green and blue channels, respectively.

Both composite RGB images were produced for several regions of interest (ROIs) over the 5 sites described in Section 3. More specifically, for each CRISM product over these sites, at least one depression rim and one area of featureless ice was selected for further analysis. In the case of Site 4, a curl feature was also examined to incorporate Unit A1. The ROIs all contain a minimum of 20 pixels in order to reduce the effects of outliers and noise. Finally, statistics for each ROI were generated through ENVI, while minimum and maximum values were recorded to compare variation in spectral reflectance across each ROI

ROI band thresholds were used to identify the strongest 10% of CO_2 and H_2O ice signatures from each scene, and then ROIs of a minimum of 20 pixels chosen from the same across-track region of the scene as the dark-rim features to provide local 'purest' ice spectra while minimising across track 'smile' effect and changes in observation conditions. Both library and local spectra can be used to compare more ambiguous spectra and identify diagnostic features. On the basis of minerals mentioned in Yung et al. (2010), the Viviano-Beck et al. (2014) library spectra for jarosite ($KFe_3^{+3}[OH]_6[SO_4]_2$), magnesium carbonate ($MgCO_3$), magnesium-rich olivine ($[Mg^{+2}, Fe^{+2}]_2SiO_4$), high-calcium pyroxene ($Ca_2Si_2O_6$), magnesium rich smectite clays, and talc ($H_2Mg_3[SiO_3]_4$) are of particular interest to this study.

5. Results

Fig. 5 shows an example of the spectral difference between the SPRC and the surrounding area for Site 1. The left panel shows the "true colour" RGB composite while the right panel shows the RGB composite summary product. The regolith area is dark purple in colour in the right hand image, indicating a strong response for the carbonate overtone-like summary product (blue) and some CO_2 ice, possibly in the form of permafrost within the regolith. The margin of the SPRC is turquoise, indicating a mix of water and CO_2 ice, as would be expected from a higher water ice content (green) at the edge of the SPRC described by Thomas et al. (2009). The SPRC itself in the bottom left of the panel shows the higher CO_2 content typical of the SPRC.

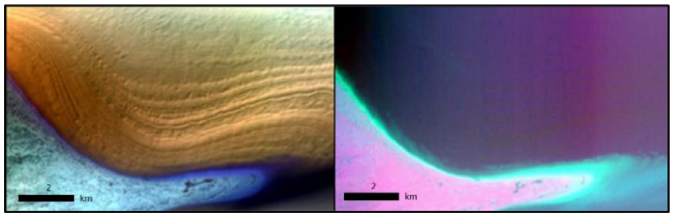

Fig. 5. Left: False colour visualisation of Site 1 (FRT00007E26) from CRISM bands R = 230 G = 75 B = 10. Right: False colour visualisation of Site 1 using Pelkey (2007) summary products R = 1435 (CO_2 ice) G = 1500 (H_2O ice) B = BDCARB (carbonate overtones).

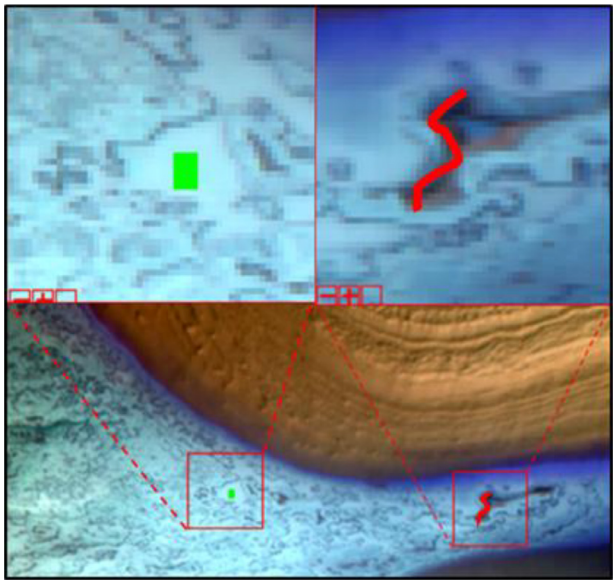

Fig. 6. Locations and close ups of Site 1 (FRT00007E26), ROI A (red line, Dark Rim) and B (green rectangle, Featureless Ice). Red squares are 1 × 1 km. (For interpretation of the references to colour in this figure legend, the reader is referred to the web version of this article.)

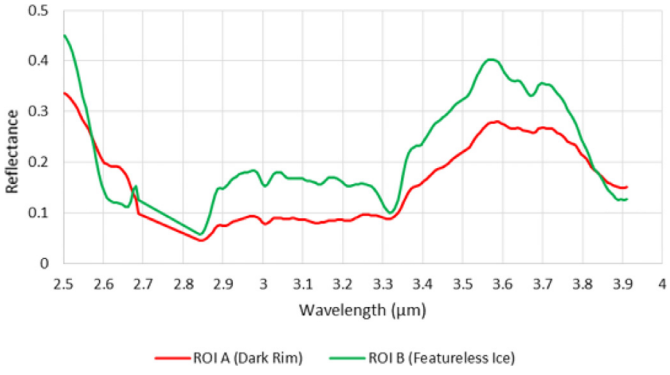

Fig. 7. Reflectance spectra of ROIs A, B (Site 1).

The Regions of interest (ROIs) incorporate all pixels intersected or covered by the polyline or rectangle (though polyline has been made bolder in Fig. 6 for visibility). ROI A (red line) is situated on a large depression feature, while ROI B (green rectangle) is a featureless patch of ice on the CO_2 rich SPRC, away from the water ice rich margin. These are both shown in Fig. 6. ROI B exhibits a wider variation in minimum and maximum reflectance values within the spectrum than ROI A, as is shown in Fig. 7.

Fig. 7 shows the lower overall reflectance values of ROI A in comparison to ROI B, a consequence of the lower albedo of the dust covered, textured scarp features, and because of possible lower solar irradiance in the topographically low shadowed rims. The trough just above 3.3 µm is much more pronounced in featureless ice.

At Site 2, the spectral mapping demonstrated scarp features in shadow correspond to carbonate overtones summary products, whereas the illuminated scarps correspond to water ice. This difference between shadowed and illuminated areas is unlikely to be due to any actual compositional difference, but to the spectral response differences caused by sunlight in areas with higher reflectance values.

Site 2 reveals greater variation in minimum and maximum reflectance at ROIs A and B, situated on Dark Rims than on the mesa plateau (ROI C). Variation was greatest at ROI A, the scarp that was highlighted as possibly suggestive of carbonates by the RGB composite summary products. When compared, the spectra of ROI 2B and ROI 2C are virtually identical. It is clear that the illumination angle of the scarps results in different reflectance values between ROI 2A and those of ROI 2B and 2C.

Site 3 exhibits Dark Rims around most depressions and mesas independent of illumination angle. The dark rims largely indicate water ice. Four ROIs were selected for this region. ROI 3A is a dark rim that shows strong signals for the carbonate overtone summary product parameters, while ROI 3C is from a mesa scarp and indicates water ice content. ROIs 3B and 3D are from a mesa plateau and featureless patch of ice respectively, and exhibit indications of higher CO_2 content.

Examination of ROIs 3A and 3C once again implies that Dark Rim regions show greater variation between minimum and maximum reflectance within the spectra while ROIs 3B and 3D show very little variation within the spectra. Moreover, the spectral profiles of flat, icy regions (ROIs B and D) are very similar. On the other hand, there is a rise in differences in reflectance between ROI 3A and ROI 3C beyond 3.4 µm, but overall the spectral profiles are similar. Finally, the dark rims show a broader, shallower absorption feature at 3 µm compared to the absorption feature for non-rim ROIs 3B and 3D.

Regarding Site 4, ROI 4A is taken from the edge of a curled feature, while ROI 4B is within a curl feature. ROI 4C is situated on a featureless patch of ice between the curl features. As with the Dark Rim spectra from previous sites, the curl feature rim from ROI 4A exhibits greater variation in minimum and maximum reflectance values compared with smooth ice features. While there is less variation within the curl than at its edge, ROI 4B still shows greater min/max reflectance variation than ROI 4C.

Despite differences in minimum and maximum reflectance variation, the curl feature (ROI 4B) and the featureless ice (ROI 4C) have virtually identical spectral profiles; the Dark Rim of the curl feature (ROI 4A) has an overall lower reflectance.

Four ROIs were investigated at Site 5. Similar to the previous investigation sites, there is higher variability in reflectance on Dark Rim ROIs and much more consistent reflectance across all pixels in ROIs B and D.

Finally, similar to Site 3, the illuminated dark rim (ROI 5C) that showed strong signatures for the water ice summary product, shows a very similar spectral profile to the mesa and featureless patch of ice (ROIs 5B and 5D) while the dark rim in shadow (ROI 5A) exhibits lower overall reflectance.

6. Analysis and discussion

The initial results show that Dark Rim sites consistently show a much wider variation in minimum and maximum reflectance across all ROI pixels than ROIs in Non-Rim locations. Moreover, when the spectral profiles of all Dark Rims from all sites are plotted together, they display a large range of reflectance levels (Fig. 8). However, the spectral profiles of all Non-Rim areas are somewhat more consistent with each other, particularly above 3.4 µm (Fig. 9).

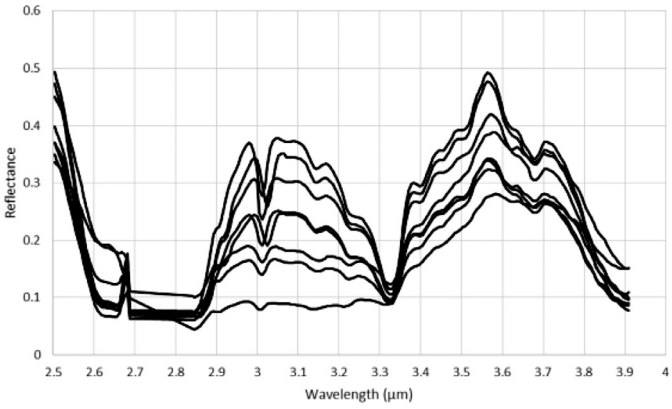

Fig. 8. Reflectance spectra of all Dark Rim ROIs from all 5 sites.

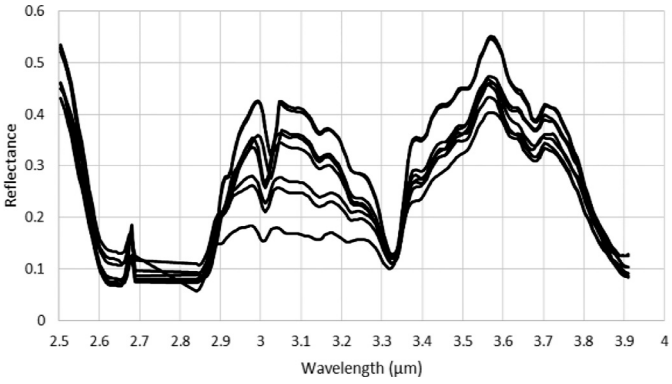

Fig. 9. Reflectance spectra of Non-Rim ROIs from all 5 sites.

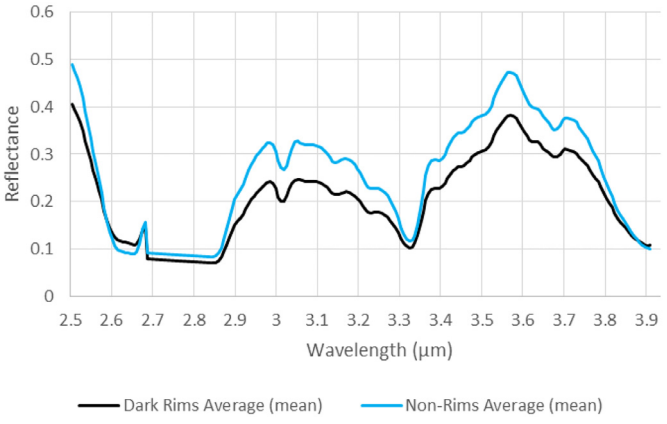

Fig. 10. Average spectra of Dark Rim and Non-Rim ROIs for all 5 sites.

In order to further analyse the overall characteristics of Dark Rim and Non-Rim regions, mean spectra were produced by averaging all rim spectra from Fig. 8 for Dark Rims, and all Non-Rim spectra from Fig. 9, to create two new spectral profiles (Fig. 10).

Averaging the spectra of all regions is not particularly useful for examining individual, subtle characteristics of Dark Rim features, as any unique features will be lost. However, the average Dark-Rim and Non-Rim spectra are useful for looking at the effects of water and CO_2 ice on spectral profiles.

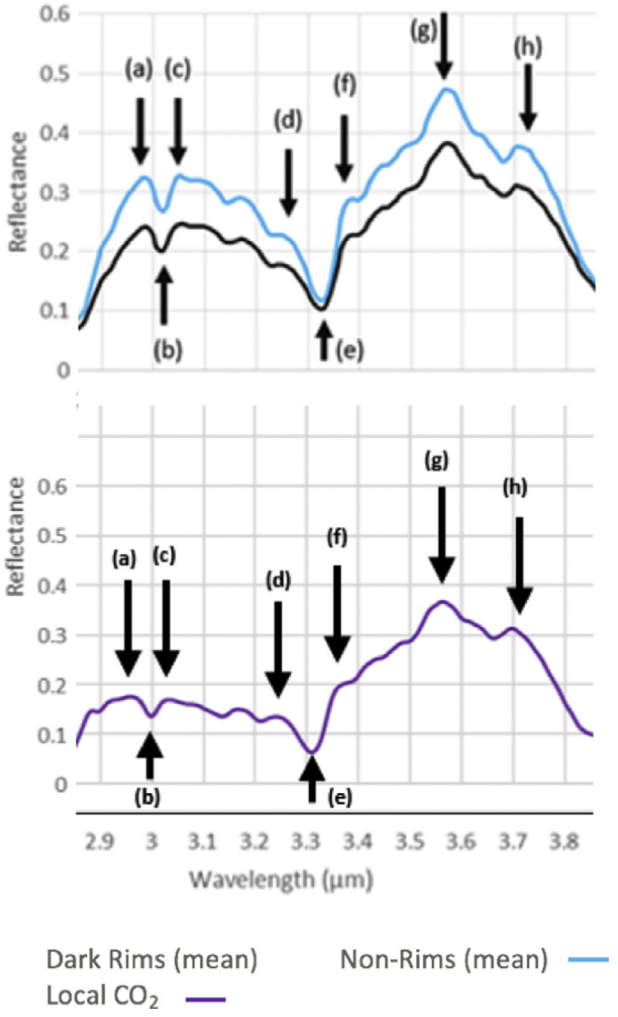

Fig. 11. Comparison of peaks and troughs between average spectra of Dark Rims and Non-Rims (black and blue) and mean strongest 10% of local CO_2 summary product spectra (purple). (For interpretation of the references to colour in this figure legend, the reader is referred to the web version of this article.)

6.1. CO_2 ice spectral features

Given that the SPRC is dominated by CO_2 ice, removing the spectral features of CO_2 ice from the ROI spectra enables residual features to be more effectively analysed. Fig. 11 shows the spectral profile for local CO_2 ice below the average spectra of the two types of ROI from Fig. 10.

Features from the local CO_2 spectrum appear in the ROI spectra. The local 10% threshold ROI spectra (in purple) show a more similar profile to the rim and non-rim regions. Fig. 11 highlights 8 peaks and troughs from the local CO_2 spectra that correlate with features in the Dark Rim and Non-Rim averaged spectra. The 8 peaks and troughs (a-h) are only the most obvious features that can be seen on both the CO_2 and average ROI spectra to glean an overall idea of common distinctive attributes.

It would appear that CO_2 signatures contribute significantly to the Dark-Rim ROIs; this is to be expected in such a CO_2 ice rich environment. It is clear there is a difference in overall reflectance values between Dark Rim and Non-Rim regions, which is likely to be a consequence of the lower albedo of the darker, textured scarp surfaces (Byrne, 2009).

The overwhelming influence of the CO_2 content of the ROIs must be removed in order to see any subtler compositional characteristics. In order to minimise the effects of CO_2 ice, the values for the two types of ROI were divided by local CO_2 spectra.

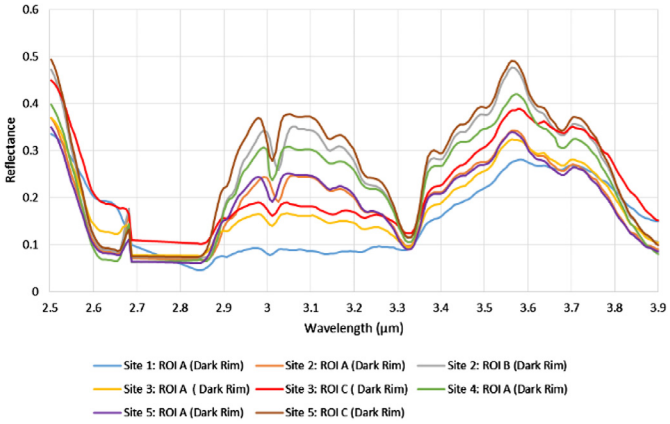

Fig. 12. Spectral profiles of all Dark Rim ROIs.

6.2. H_2O ice spectral features

Further processing of the ROI spectra may be necessary to highlight differences between Dark Rims and Non-Rims. Back-wasting of scarps can expose higher concentrations of H_2O ice inside depressions (Thomas et al., 2009), and so it was prudent to attempt to account for the effects of water ice on ROI spectra to see if the rims are composed of more water ice than Non-Rims.

ROI thresholds for the strongest 10% of H_2O summary product parameters were used to obtain diagnostic water-ice rich spectra. The results showed no discernible effect on the wavelengths of interest, with the local water ice rich regions still being largely overwhelmed by CO_2 ice signatures.

Identification of PAH-like signatures on Iapetus and Phoebe relied on ice-free surface deposits of material; the Martian SPRC has no such extensive regions of low albedo material. The very small surface area of the depression scarps mean that the dust content is likely to be very low, and any organics would be present in even lower concentrations. This problem is further exacerbated by the ~20 m spatial resolution of the CRISM instrument, which cannot resolve uninterrupted dark patches, and will almost always encompass some area of dust-free, icy surface material.

The presence of strong spectral responses of a CO_2 ice makes it very difficult to identify any weak absorption features that might be present at ~3.3 μm. The averaged ROI spectra by their very nature smooth out unique features. While these generic spectra have been useful in establishing the overall common characteristics of Dark Rim and Non-Rim ROIs, and ascertaining the impact of water and CO_2 ice spectra on ROI features, it is necessary to examine individual ROIs for absorption features at ~3.3 μm.

6.3. Analysis of individual spectra

Fig. 12 shows all the spectral profiles of the Dark Rims ROIs. The 3 ROIs with the lowest reflectance in the PAH region of interest were chosen in order to minimise the effects of the impact of the steep shoulder into the CO_2 ice absorption feature at just above 3.3 μm. They are ROI A from Site 1, and ROIs A and C from Site 3. The Non-Rim features from the same sites are also analysed in order to examine the spectral differences of regions within the same CRISM scene.

These 3 Dark Rim sites are also interesting as they exhibit dark coverage around the whole rim regardless of illumination angle, suggesting dust coverage rather than simply shadow. Future work

will involve 3D modelling of SCT features in order to mitigate this effect.

In order to ascertain subtle differences between the two ROIs, PeakFit software (http://www.sigmaplot.co.uk/products/peakfit) was used to carry out a statistical fit to accentuate peaks. Corrected rim and non-rim profiles were compared to CO_2 and water ice as well as the 6 minerals of interest from Section 4.3 (jarosite, magnesium carbonate, magnesium-rich olivine, high-calcium pyroxene, magnesium rich smectite clays, and talc).

Whilst there is an overall difference in reflectance intensity, with ROI B being more reflective, both regions show 8 peaks in very similar regions, indicating no significant compositional difference.

The Gaussian decomposition of Dark Rim ROI 3A revealed far more individual peaks, with 17 distinct features, compared with the mesa plateau of ROI B, which only shows 11, suggesting a significant compositional difference between the two regions.

Moreover, once corrected for CO_2 ice and subjected to Gaussian decomposition, some significant differences arise. After comparison with the 6 minerals of interest, there is a similarity between ROI A and the spectrum for magnesium carbonate; while only several peaks match carbonate features and does not definitively identify carbonates, the presence of these peaks is consistent with the results from spectral mapping in that we have identified ROI A as having at least some features similar to that of carbonate overtones.

As with Site 3 ROIs 3A and 3B, ice correction of spectra highlights a compositional difference between ROI 3C and 3D. The spectral map of Site 2 highlighted ROI C as water-ice rich, and this is consistent with the weaker carbonate peaks when compared with Site 3, ROI A.

7. Conclusions and future work

PAHs are crucial to theories of abiogenesis, and despite their ubiquitous presence in space, their detection on planetary bodies remains a primary objective for the field of planetary science. The attempt to identify them on Mars is important given the recent discoveries of other organic compounds and possible liquid water (Freissinet et al., 2015; Ojha et al., 2015). The ability to critically analyse the influence of CO_2 and H_2O ice spectra on ROIs has paved the way for further in-depth analysis of spectral features of dust rims.

Spectral mapping has revealed that there is a distinct compositional difference between the majority of the SPRC and depression rims for all morphological units. Further analysis of ROI spectral features reveals the compositional differences are highlighted when spectra are corrected for interference from ices.

Dark Rims exhibit more variation in reflectance within spectra than Non-Rims. The influence of water ice is greater on rims and once removed, Dark Rim spectra more closely resemble the spectra of Non-Rims. CO_2 ice is a limiting factor due to the strong absorption feature between 3.3 and 3.4 µm, while water ice appears to have less of an impact.

In the future, other spectrometers such as TES and OMEGA will be used to further examine Dark Rims, even though all current Mars orbital spectrometers are limited by spatial resolution, thus impeding the analysis of ice free pixels. Moreover, further analysis of the SPRC is planned, during which many more ROIs will be examined, and more CRISM products from multiple MY will be included, in order to monitor temporal changes in spectra. 3D modelling of SCT features will also enable the mitigation of the effects of solar illumination angle on spectral response, and laboratory experiments are being carried out to examine the impact of different mixtures of Mars analogue soil samples and PAHs on CO_2 spectra, with further computer modelling planned using these laboratory measurements.

It is possible that the non-targeted CRISM modes (which have global coverage) could be composited over time to analyse the entire SPRC, as FRT only has 1% surface coverage, and much of the SPRC has not been imaged at high resolution. The 100–200 m spatial resolution of non-targeted mode may exclude effective perusal of small-scale features, but may be useful to map larger regions, and for use in conjunction with data from more holistic data such as that from MARCI (Bell et al., 2009), in order to ascertain if there is any relationship between the wider Martian climate and the spectral evolution of SCT features.

PAHs have not been detected to the sensitivity level of the CRISM instrument, but this study has revealed tantalising details about the composition of the Martian SPRC, and how to effectively identify dust components; it has far reaching consequences for other planetary bodies such as Europa, Enceladus and Titan, the study of which would greatly benefit from being able to eliminate the effects of ice on spectra, and comparison with PAH libraries. Identifying PAHs on Mars is a unique challenge as the dynamics of CO_2 and water ice also conspire to mask PAH signatures, and given that the atmosphere is largely missing on other outer planet bodies, this may play a part in obscuring their signatures.

Overall, no direct evidence of PAHs was found but the search continues.

Acknowledgements

The first author acknowledges support from STFC under studentship number 526933. This work forms part of the European Union's Seventh Framework Programme (FP7/2007-2013) under iMars grant no. 607379 and partial funding was obtained from the STFC "MSSL Consolidated Grant" ST/K000977/1. Gratitude is also expressed to the CRISM team.

Supplementary materials

Supplementary material associated with this article can be found, in the online version, at doi:10.1016/j.icarus.2018.03.008.

References

Africano, J., Kervin, P., Hall, D., Sydney, P., Ross, J., Payne, T., Gregory, S., Jorgensen, K., Jarvis, K., Parr-Thumm, T., Stansbery, G., Barker, E., 2005. Understanding photometric phase angle corrections. In: Proceedings of the 4th European Conference on Space Debris, pp. 141–146.

Allamandola, L.J., 2011. PAHs and astrobiology. In: PAHS and the Universe, 46, pp. 305–317. EAS Publications Series.

Allamandola, L.J., Tielens, A.G, Barker, J.R., 1985. Polycyclic aromatic hydrocarbons and the unidentified infrared emission bands: auto exhaust along the Milky Way!. Astrophys. J. 290, 25–28.

Bell, J.F., Wolff, M.J., Malin, M.C, Calvin, W.M., Cantor, B.A, Caplinger, M.A., Clancy, R.T, Edgett, K.S, Edwards, LJ, Fahle, J., Ghaemi, F., Haberle, R.M., Hale, A, James, P.B, Lee, S.W, McConnochie, T., Noe Dobrea, E., Ravine, M.A., Schaeffer, D., Supulver, K.D, Thomas, P.C., 2009. Mars reconnaissance orbiter mars color imager (MARCI): instrument description, calibration, and performance. J. Geophys. Res. 114, E08S92. doi:10.1029/2008JE003315.

Benner, S.A., Devine, K.G., 2000. The missing organic molecules on Mars. Proc. Natl. Acad. Sci. 97, 2425–2430.

Bibring, J.P., Langevin, Y., Poulet, F., Gendrin, A., Gondet, B., Berthe, M., Soufflot, A., Drossart, P., Comes, M., Bellicci, G., Moroz, V., Mangold, N., Schmitt, B.and the OMEGA Team, 2004. Perennial water ice identified in the south polar cap of Mars. Nature 428, 627–630.

Blackburn, D.G., Bryson, K.L., Chevrier, V.F., Roe, L.A., White, K.F., 2010. Sublimation kinetics of CO_2 ice on Mars. Planet. Space Sci. 58, 780–791.

Botta, O., Bada, J., 2002. Extraterrestrial organic compounds in meteorites. Surv. Geophysics. 23, 411–467.

Byrne, S., 2009. The polar deposits of Mars. Annu. Rev. Earth Planet. Sci. 37, 535–560.

Byrne, S., Russel, P.S., Fishbaugh, K.E., Hansen, C.J., Herkenhoff, K.E., McEwan, A.S. HiRISE Team, 2008. Explaining the persistence of the southern residual cap of Mars. HiRISE data and landscape evolution models. Lunar Planet. Sci. 39, 2252.

Carey, F.A., 2006. Organic Chemistry. McGraw Hill, pp. 457–459.

Cockell, C.S., Catling, D.C., Davis, W.L., Snook, K., Kepner, R.L., Lee, P., McKay, C.P., 2000. The ultraviolet environment of Mars: biological implications past, present and future. Icarus 146, 343–359.
Colangeli, L., Mennella, V., Baratta, G.A., Bussoletti, E., Strazzulla, G., 1992. Raman and infrared spectra of polycyclic aromatic hydrocarbon molecules of possible astrophysical interest. Astrophys. J. 396, 369–377.
Cruikshank, D.P., Dalle Ore, C.M., Clark, R.N., Pendleton, Y.J., 2014. Aromatic and aliphatic organic materials on Iapetus: analysis of Cassini VIMS data. Icarus 233, 306–315.
Cruikshank, D.P., Wegryn, E., Dalle Ore, CM., Brown, R.H., Bibring, J-P., Buratti, B.J., Clark, R.N., McCord, T.B., Nicholson, P.D., Pendleton, Y.J., Owen, T.C., Filacchione, G., Coradini, A., Cerroni, P., Capaccioni, F., Jaumann, R., Nelson, R.M., Baines, K.H., Sotin, C., Bellucci, G., Combes, M., Langevin, Y., Sicardy, B., Matson, D.L., Formisano, V., Drossart, P., Mennellao, V., 2008. Hydrocarbons on Saturn's satellites Iapetus and Phoebe. Icarus 193, 334–343.
Dartnell, L.R., Patel, M.R., Storrie-Lombardi, M.C., Ward, J.M., Muller, J.P., 2012. Experimental determination of photostability and fluorescence-based detection of PAHs on the Martian surface. Meteorit. Planet. Sci. 47 (5), 806–819.
Davidsson, B.J.R., Sierks, H., Guttler, C., Marzari, F., Pajola, M., Rickman, H., AHearn, M.F., Auger, A.T., El-Maarry, M.R., Fornasier, S., Gutierrez, P.J., Keller, H.U., Massironi, M., Snodgrass, C., Vincent, J.B., Barbieri, C., Lamy, P.L., Rodrigo, R., Koschny, D., Barucci, M.A., Bertaux, J.L., Bertini, I., Cremonese, G., Da Deppo, V., Debei, S., De Cecco, M., Feller, C., Fulle, M., Groussin, O., Hviid, S.F., Hofner, S., Ip, W.H., Jorda, L., Knollenberg, J., Kovacs, G., Kramm, J.R., Kuhrt, E., Kuppers, M., La Forgia, F., Lara, L.M., Lazzarin, M., Lopez-Moreno, J.J., Moissl-Fraund, R., Mottola, S., Naletto, G., Oklay, N., Thomas, N., Tubiana, C., 2016. The primordial nucleus of comet 67P/Churyumov-Gerasimenko. Astron. Astrophys. 592, A63.
Douté, S., Schmitt, B., Langevun, Y., Bibring, J-P., Altieri, F., Bellucci, G., Condet, B., Poulet, F., 2007. South Pole of Mars: nature and composition of the icy terrains from Mars Express OMEGA observations. Planet. Space Sci. 55, 1–2 113-133.
Dullemond, P., Henning, T.H., Visser, R., Geers, V.C., van Dishoeck, E.F., Pontoppidan, K.M., 2007. Dust sedimentation in protoplanetary disks with polycyclic aromatic hydrocarbons. Astron. Astrophys. 473, 457–466.
ESA Robotic Exploration of Mars: The ExoMars Drill Unit (on-line) Accessed 20 January 2016. http://exploration.esa.int/mars/43611-rover-drill/.
Fairén, A.G., Davila, A.F., Lim, D., Bramall, N., Bonaccorsi, R., Zavaleta, J., Uceda, E.R., Stoker, C., Wierzchos, J., Dohm, J.M., Amils, R., Andersen, D., McKay, C.P., 2010. Astrobiology through the ages of Mars: the study of terrestrial analogues to understand the habitability of Mars. Astrobiology. 10 (8), 821–843.
Fassett, C.I., Head, J.W., 2010. Sequence and timing of conditions on early Mars. Icarus. 211, 1204–1214.
Freissinet, C, Glavin, D.P, Mahaffy, P.R., Miller, K.E., Eigenbrode, J.L., Summons, R.E., Brunner, A.E., Buch, A., Szopa, C., Archer Jr., P.D., Franz, H.B., Atreya, S.K., Brinckerhoff, W.B., Cabane, M., Coll, P., Conrad, P.G., Des Marais, D.J., Dworkin, J.P., Fairén, A.G., François, P., Grotzinger, J.P., Kashyap, S., ten Kate, I.L., Leshin, L.A., Malespin, C.A., Martin, M.G., Martin. Torres, F.J., McAdam, A.C., Ming, D.W., Navarro-González, R., Pavlov, A.A., Prats, B.D., Squyres, S.W., Steele, A., Stern, J.C., Sumner, D.Y., Sutter, B., Zorzano, M.-P.The MSL Science Team, 2015. Organic molecules in the Sheepbed Mudstone, Gale Crater, Mars. J. Geophys. Res.: Planets 120 (3), 495–514.
Gaffey, S.J., 1986. Spectral reflectance of-carbonate minerals in the visible and near infrared (0.35-2.55 microns): calcite, aragonite, and dolomite. Am. Mineral. 71, 151–162.
Hecht, M.H., Kounaves, S.P., Quinn, R.C., Wes, S.J., Young, S.M.M., Ming, D.W., Catling, D.C., 2009. Detection of perchlorate and the soluble chemistry of Martian soil at the phoenix lander site. Science. 325 (5936), 64–67.
Herbst, E., van Dishoek, E.F., 2009. Complex organic interstellar molecules. Annu. Rev. Astron. Astrophys. 47, 427–480.
Herr, K.C., Forney, P.B., Pimmental, G.C., 1972. Mariner Mars 1969 infrared spectrometer. Appl. Opt. 11, 493–501.
Jian, J.J., Ip, W.H., 2009. Seasonal patterns of condensation and sublimation cycles in the cryptic and non-cryptic regions of the South Pole. Adv. Space Res. 43, 138–142.
Johnson, R.E., Liu, M., Kass, D.M., Yung, Y.L., 1996. The loss of atmosphere from Mars. Science 274, 1932–1933.
Kass, D.M., Yung, Y.L., 1995. Loss of atmosphere from Mars due to solar wind-induced sputtering. Science 268, 697–699.
Klein, H.P., 1978. The viking biological experiments on Mars. Icarus. 34 (3), 666–674.
Leger, A., Puget, J.L., 1984. Identification of the 'unidentified' IR emission features of interstellar dust? Astron. Astrophys. 137 (1), 5–8.
Lopez-Puertas, M., Dinelli, B.M., Adriani, A., Funke, B., Garcia-Comas, M., Moriconi, M.L., D'Aversa, E.D., Boersma, C., Allamandola, L.J., 2013. Large abundances of polycyclic aromatic hydrocarbons in Titan's upper atmosphere. Astrophys. J. 770 (132), 1–8.
Malin, M.C., Caplinger, M.A., Davis, S.D., 2001. Observational evidence for an active surface reservoir of solid carbon dioxide on Mars. Science 294, 2146–2148.
McKay, D., Gibson, E., 1996. Search for past life on Mars; possible relic biogenic activity in Martian meteorite ALH84001. Science 273, 924–930.
Melosh, H.J., Vickery, A.M., 1989. Impact erosion of the primordial atmosphere of Mars. Nature 338, 487–489.
Morgan, F., Seelos, F., Murchie, SThe CRISM Team CRISM Data Users' Workshop CAT Tutorial (on-line). NASA/JPL/John Hopkins University Accessed 23 January 2016. http://pds-geosciences.wustl.edu/missions/mro/CRISM_Workshop_090322_CAT_MFM.pdf.
Mulas, G., Malloci, C., Joblin, C., Toublanc, D., 2005. Estimated IR and phosphorescence emission fluxes for specific polycyclic aromatic hydrocarbons in the Red Rectangle. Astron. Astrophys. 446, 537–549.
Murchie, S., Arvidson, R., Bedini, P., Beisser, K., Bibring, J-P., Bishop, J., Boldt, J., Cavender, P., Choo, T., Clancy, R.T., Darlington, E.H., Des Marais, D., Espiritu, R., Fort, D., Green, R., Guinness, E., Hayes, J., Hash, C., Heffernan, K., Hemmler, J., Heyler, G., Humm, D., Hutcheson, J., Izenberg, N., Lee, R., Lees, J., Lohr, D., Malaret, E., Martin, T., McGovern, J.A., McGuire, P., Morris, P., Mustard, J., Pelkey, S., Rhodes, E., Robinson, M., Roush, T., Schaefer, E., Seagrave, G., Seelos, F., Silverglate, P., Slavney, S., Smith, M., Shyong, W.J., Strohbehn, K., Taylor, H., Thompson, P., Tossman, B., Wirzburger, M., Wolff, M., 2007. Compact Reconnaissance Imaging Spectrometer for Mars (CRISM) on Mars Reconnaissance Orbiter (MRO). J. Geophys. Res. 112, E05S03. doi:10.1029/2006JE002682.
NASA/JPL. (2016). Mars Reconnaissance Orbiter: Mission Instruments: CRISM (on-line). NASA Accessed 24 March 2016. http://mars.jpl.nasa.gov/mro/mission/instruments/CRISMcompactreconnaissanceimagingspectrometerformars.
Navarro-González, R., Vargas, E., de la Rosa, J., Raga, A.C., McKay, C.P., 2010. Reanalysis of the Viking results suggests perchlorate and organics at mid-latitudes on Mars. J. Geophys. Res.: Planets 115, E12. doi:10.1029/2010JE003599.
Oberg, K.I., Garrod, R.T., van Dishoek, E.F., Linnartz, H., 2009. Formation rates of complex organics in UV irradiated CH_3OH-rich ices. Astron. Astrophys. 504 (3), 891–913.
Ojha, L., Willhelm, M.B., Murchie, S.L., MEwen, S.S., Wray, J.J., Hanley, J., Masse, M., Chojnacki, M., 2015. Spectral evidence for hydrated salts in recurring slope lineae on Mars. Nat. Geosci. 8, 829–832.
Paige, D., Herkenhoff, K., Murray, B., 1990. Mariner 9 observations of the south polar cap of Mars: evidence for residual CO_2 frost. J. Geophys. Res. 95, 1319–1335.
Pelkey, S.M., Mustard, J.F., Murchie, S., Clancy, R.T., Wolff, M., Smith, M., Milliken, R., Bibring, J.P., Gendrin, A., Poulet, F., Langevin, Y., Gondet, B., 2007. CRISM multispectral summary products: parameterizing mineral diversity on Mars from reflectance. J. Geophys. Res. 112, E08S14. doi:10.1029/2006JE002831.
Piqueux, S., Edwards, C.S., Christensen, P.R., 2008. Distribution of the ices exposed near the south pole of Mars using THEMIS temperature measurements. J. Geophys. Res. 113, E02006.
Pommerol, A., Portyankina, G., Tomas, N., Aye, K-M., Hansen, C.J., Vincendon, M., 2011. Evolution of the south seasonal cap during Martian spring: insights from the high-resolution observations by HiRISE and CRISM on Mars Reconnaissance Orbiter. J. Geophys. Res. 116, 898–910.
Quinn, R., Zent, A., 1999. Peroxide-modified titanium dioxide: a chemical analogue of putative Martian soil oxidants. Orig. Life Evol. Biospheres 29, 59–72.
Samanta, S.K., Singh, O.V., Jain, R.K., 2002. Polycyclic aromatic hydrocarbons: environmental pollution and bioremediation. Trends Biotechnol. 20 (6), 243–248.
Schuerger, A.C., Clark, B.C., 2007. Viking biology experiments: lessons learned and the role of ecology in future Mars life-detection. Space Sci. Rev. 135. doi:10.1007/s11214-007-9194-2.
Thomas, P.C., James, PB., Calvin, W.M., Haberle, R., Malin, M.C., 2009. Residual south polar cap of Mars: stratigraphy, history, and implications of recent changes. Icarus 203, 352–375.
Thomas, P.C., Malin, M.C., James, P.B., Cantor, B.A., Williamns, R.M.E., Gierasch, P., 2005. South polar residual cap of Mars: features, stratigraphy, and changes. Icarus 174, 535–559.
Titus, T.N., Kieffer, H.H., Christensen, P.R., 2003. Exposed water ice found near the south pole of Mars. Science 299, 1048–1051.
Titus, T.N., Prettyman, T.H., Winfree, K.N., 2006. How thick is the south polar residual cap CO_2 ice cover? In: LPI Contributions. 4th Mars Polar Science Conference, 1323, p. 8054.
Tokunga, A.T., Sellgren, K., Smith. Nagata, T., Sakata, A., Nakada, Y., 1991. High-resolution spectra of the 3.29 micron interstellar emission feature: a summary. Astrophys. J. 380, 452–460.
Vincent, W.F., Rae, R., Laurion, I., Howard-Willimans, C., Priscu, J.C., 1998. Transparency of Antarctic ice-covered lakes to solar UV radiation. Limnol. Oceanogr. 43 (4), 618–624.
Viviano-Beck, C.E., et al., 2014. Revised CRISM spectral parameters and summary products based on the currently detected mineral diversity on Mars. J. Geophys. Res. Planets 119, 1403–1431.
Wiseman, S.M., Arvidson, R.E., Wolff, M.J., Smith, M.D., Seelos, F.P., Morgan, F., Murchie, S.L., Mustard, J.F., Morris, R.V., Humm, D., McGuire, P.C., 2016. Characterisation of artifacts introduced by the empirical volcano-scan atmospheric correction commonly applied to CRISM and OMEGA near infrared spectra. Icarus 269, 111–121.
Yung, Y.L., Russell, M.J., Parkinson, C.D., 2010. The search for life on Mars. J. Cosmol. 5, 1121–1130.
Zolotov, M., Shock, E., 1999. Abiotic synthesis of PAHs on Mars. J. Geophys. Res. 104, 1433–1449.